Multidimensional Born Inversion with a Wide-Band Plane Wave Source

Cengiz Esmersoy

Department of Electrical Engineering and Computer Science
and
Earth Resources Laboratory
Department of Earth, Atmospheric and Planetary Sciences
Massachusetts Institute of Technology, Cambridge, Massachusetts 02139

Bernard C. Levy[a)]

Department of Electrical Engineering and Computer Science
Massachusetts Institute of Technology, Cambridge, Massachusetts 02139

ABSTRACT

The inverse scattering problem for an acoustic medium is considered within the homogeneous background Born approximation. A constant density acoustic medium is probed by a wide-band plane wave source. The scattered field is observed along a receiver array located outside the medium. Two methods for partial reconstruction of the medium velocities are presented. In the first method (the slant-stack method), the projections of the velocity potential at a range of angles are obtained from the plane-wave components of the scattered field. The range of available projection angles is determined by the receiver array aperture and the incidence direction of the probing plane wave. The medium velocities are, then, partially reconstructed from available projections via well-known methods of straight-line tomography. In the second method (the imaging-filtering method), the observed traces are filtered, back-propagated into the medium and imaged at the source travel times, in the same way as in migration. The resulting image is, then, filtered by a linear space-invariant filter to obtain a partial reconstruction of the medium velocities. Both reconstruction methods

are illustrated by some synthetic examples for several receiver geometries.

1. Introduction

Consider the scattering experiment described in Figure 1. A constant density acoustic medium is probed by a wide-band plane wave and the scattered field is observed along a receiver array. Then, the Fourier transform $P(\underline{x},\omega)$ of the pressure field satisfies

$$[\ \nabla^2 + k^2 n^2(\underline{x})\ ]\ P(\underline{x},\omega) = 0\ , \tag{1}$$

where $k = \omega / c$ is the wavenumber, c is a reference velocity, and if $v(\underline{x})$ denotes the medium velocity function, $n(\underline{x}) = c / v(\underline{x})$ is the refraction index measured with respect to the velocity c. Throughout this paper, it will be assumed that the velocities $v(\underline{x})$ do not deviate significantly either in value or in extent from the background velocity c, so that

$$n^2(\underline{x}) = 1 + \gamma(\underline{x})\ , \tag{2}$$

where the scattering potential $\gamma(\underline{x})$ is small with respect to unity. By substituting (2) inside (1), we can rewrite equation (1) as

$$[\ \nabla^2 + k^2\ ]\ P(\underline{x},\omega) = -k^2\ \gamma(\underline{x})\ P(\underline{x},\omega)\ , \tag{3}$$

where the operator $\mathbf{D}_0 = \nabla^2 + k^2$ appearing on the left hand side of (3) is a constant unperturbed Helmholtz operator, and where the forcing term on the right hand side can be viewed as a small perturbation. The solution of (3) can be expressed as

$$P(\underline{x},\omega) = P_0(\underline{x},\omega) + k^2 \int_V d\underline{x}'\ \gamma(\underline{x}')\ P(\underline{x}',\omega)\ G_0(\underline{x},\underline{x}',\omega)\ , \tag{4}$$

where the incident field $P_0(\underline{x},\omega)$ is a solution of the homogeneous equation $\mathbf{D}_0 P_0(\underline{x},\omega) = 0$, and where the second term in (4) is obtained by superposition by using the Green's function $G_0(\underline{x},\underline{x}',\omega)$ associated to $\mathbf{D}_0$. In the above equation, V is a volume enclosing the domain where $\gamma(\underline{x})$ is nonzero. For the experiment geometry considered here, the medium is probed by a plane wave, so that the incident field $P_0(\underline{x},\omega) = e^{i\underline{k}_s \cdot \underline{x}}$, where $\underline{k}_s$ is the incident plane-wave vector. Furthermore, for a two dimensional (2-D) medium

$$G_0(\underline{x},\underline{x}',\omega) = \frac{i}{4} H_0^{(1)}(k\,|\underline{x}-\underline{x}'|)\,, \tag{5a}$$

where $H_0^{(1)}(\bullet)$ denotes the Hankel function of the first kind, and for a 3-D medium

$$G_0(\underline{x},\underline{x}',\omega) = \frac{e^{ik|\underline{x}-\underline{x}'|}}{4\pi|\underline{x}-\underline{x}'|}\,. \tag{5b}$$

The main feature of equation (4) is that it is *exact*, i.e. no approximations are involved up to this point. This equation is known as the Lippmann-Schwinger equation [1], and it puts in evidence the nonlinear relation existing between the potential $\gamma(\underline{x})$ and the pressure field $P(\underline{x},\omega)$. A simple method of linearizing this equation consists in approximating the total field $P(\underline{x}',\omega)$ inside the integral in (4) by the incident field $P_0(\underline{x}',\omega)$. In this case, the scattered field $P_s(\underline{x},\omega) = P(\underline{x},\omega) - P_0(\underline{x},\omega)$ can be expressed as ([1], [2])

$$P_s(\underline{x},\omega) = k^2\, S(\omega) \int_V d\underline{x}'\, \gamma(\underline{x}')\, P_0(\underline{x}',\omega)\, G_0(\underline{x},\underline{x}',\omega)\,, \tag{6}$$

Equation (6) represents the constant background Born approximation of the scattered field, and throughout this paper we will assume it is valid. In this approximation it is assumed that the incident field $e^{i\underline{k}_s \cdot \underline{x}}$ created by the source propagates through the medium undistorted by the velocity variations. Then, each point in the medium can be viewed as a secondary point source with source

excitation given by $k^2 S(\omega)\gamma(\underline{x})e^{i\underline{k}_s \cdot \underline{x}}$ in the Fourier domain. The scattered field is constructed by the superposition of these secondary sources. Since the incident field is assumed to be independent of the velocity variations, multiple scattering effects are neglected in this model. The inversion problem considered here consists of reconstructing the scattering potential $\gamma(\underline{x})$ from observations of the scattered field at various locations outside the medium. In some cases this can be accomplished only approximately due to insufficient receiver coverage, and/or because the source has only a finite bandwidth.

The multidimensional Born inversion problem has been investigated for various observation geometries and background velocity models. The majority of the solutions which have been proposed assume a homogeneous background model, as is the case in this paper. The zero-offset reflection geometry consisting of coincident sources and receivers was considered by Cohen and Bleistein [3] for a line aperture in two dimensions, and by Norton and Linzer [4] for plane, cylindrical and spherical apertures in three dimensions. Raz [5] and Clayton and Stolt [6] considered the same experiment geometry as Cohen and Bleistein, but with unstacked data. In other words, for each source the scattered field is recorded at all receivers rather than only at the coincident receiver. They showed that both the density and bulk modulus of the acoustic medium can be recovered with this experiment. A slightly different experiment geometry has been considered in the context of diffraction tomography. The acoustic medium is probed from various directions by monochromatic plane waves and the scattered field is recorded along a line ([7], [8], [9]). From this data, which in general contains both reflected and transmitted waves, the velocities of the medium can be reconstructed partially or completely depending on the range spanned by the angles of incidence of the plane waves ([10]). The diffraction tomography formulation has been extended by Devaney and Beylkin [11] to the case of receiver array surfaces of arbitrary shapes surrounding the medium. Another scattering experiment previously considered consists of a single wide-band point source, with receivers surrounding the medium. Esmersoy et. al. [12] have shown that, in this case, the inversion problem can be reduced to a straight-line tomography problem and that the medium velocities can be reconstructed completely.

The velocity inversion problem is closely related to the reflector imaging or migration problem. The reflectors can be imaged in two steps: first the observed scattered field is extrapolated (backpropagated) into the medium. Then, the extrapolated field is imaged at every point in the medium at a time equal to the travel time of the incident field to that point. In migration the main objective is to map the locations of the reflectors. Nevertheless, at least for simple reflectors, the peak amplitudes along the imaged reflectors can be related to the local plane-wave reflection coefficients [13]. Also, Weglein [14] observed that for zero-offset reflection data the normal derivative of the inverted velocities and the migrated image were quite similar. Subsequently, it was shown by Cheng and Coen [15] that for bandlimited data these quantities are essentially the same and that one can be obtained from the other.

In this paper we consider the inversion problem with a single wide-band plane-wave source. This is the dual of the diffraction tomography problem, i.e., instead of using one frequency and all angles of incidence, we use one angle of incidence and all frequencies. We present two methods, namely the slant-stack and imaging-filtering methods, for partially reconstructing the velocity potential from the observed scattered field. First, it is shown that there is a simple map between the plane-wave component of the scattered field at a fixed angle ϑ and the projection of the potential at an angle φ which is algebraically related to ϑ and ϑ_s, where ϑ_s is the angle of incidence of the probing plane wave. Therefore, projections of the potential at various projection angles can be obtained from the plane-wave scattering amplitudes. The plane-wave scattering amplitudes are obtained from the scattered field by performing a slant-stack operation. If the receiver array does not surround the medium (incomplete coverage), only an incomplete set of projections can be obtained. For example, if the receivers are located on the surface, the available projection angles are contained in a cone of $\pi/2$. Once the projections are obtained, the velocity potential is reconstructed either by using the filtered backprojection method for the available angles, or by a multidimensional inverse Fourier transform. In both cases we set the missing projections to zero.

The imaging-filtering method consists of two steps. The first step is similar to migration. The observed traces are filtered in time, extrapolated back into the medium and imaged at the source-travel times. The velocity potential is, then, obtained by filtering this image in the spatial domain with a linear space-invariant filter. The filter is independent of the receiver array geometry, and is completely determined by the angle of incidence of the probing plane wave. Again, if the receiver coverage is incomplete, the potential can only be recovered partially. The two methods presented here are quite different conceptually and computationally. However, it can be shown that they give mathematically identical inversion results.

In the following section we discuss the slant-stack method of inversion for the general case of incomplete receiver coverage. In Sections 2.1 and 2.2 we consider the special cases of straight-line and weak-curvature receiver arrays, respectively. In Section 3 the imaging-filtering method is presented. Synthetic examples illustrating both reconstruction methods for various receiver geometries are given in Section 4.

2. Inversion by Slant-Stack

Consider the plane-wave scattering amplitude defined by

$$A(\hat{\underline{k}},\omega) = -\int_R dl\ [\ P_s(\underline{r},\omega)\ \nabla e^{-i\underline{k}\cdot\underline{r}} - \nabla P_s(\underline{r},\omega)\ e^{-i\underline{k}\cdot\underline{r}}\ ]\cdot\hat{\underline{n}}\ , \qquad (7)$$

where R is the curve along which the receivers are located, $\hat{\underline{n}}$ is the unit vector normal to R pointing towards the scatterers as shown in Figure 1, and $\underline{k} = k\hat{\underline{k}}$. The above representation of the plane-wave scattering amplitude was introduced by Devaney and Beylkin [11] for the case where the receiver array R completely surrounds the scattering medium. As such, $A(\hat{\underline{k}},\omega)$ can be viewed just as a convenient mathematical object which will be used in subsequent derivations. However, for the case of a straight-line receiver array, as indicated by equation (18) below, $A(\hat{\underline{k}},\omega)$ has also a simple physical interpretation as the plane-wave component of the scattered field which is in the direction of the unit vector $\hat{\underline{k}}$.

Furthermore, for a curved array, it can be shown that $A(\hat{k},\omega)$ is equal to the corresponding plane-wave component which would be observed by a line array normal to the direction $\hat{k}$. This justifies therefore the fact that we call $A(\hat{k},\omega)$ the plane-wave scattering amplitude for the general array geometry shown in Figure 1. The relation between the plane-wave components of the scattered field and the potential is derived in Appendix A for the case when the receivers provide only an incomplete coverage of the scattering medium. By incomplete coverage, we mean that the receiver array does not completely surround the domain V where the scattering potential $\gamma(\underline{x})$ is nonzero. It is shown that when R is an open surface asymptotic to radial lines with angles α_1 and α_2 (as indicated in Figure 1) then

$$A(\hat{k},\omega) = k^2\, S(\omega) \int_V d\underline{x}'\, \gamma(\underline{x}')\, e^{-i(\underline{k}-\underline{k}_s)\cdot\underline{x}'} \quad ; \quad \vartheta \in [\,\alpha_2\,;\,\alpha_1\,] \tag{8}$$

$$= 0 \quad ; \quad \text{otherwise}\,,$$

where ϑ is the angle corresponding to the unit vector $\hat{k}$. It is seen from this identity that, for fixed $\hat{k}$ and ω, the plane-wave amplitude is related to one point in the Fourier transform of the potential. If the receiver array surrounds the medium, we have $[\alpha_2;\alpha_1] = [0;2\pi]$ and equation (8) corresponds to the complete coverage case discussed in [11].

In the following, we will derive the relationship between the plane-wave scattering amplitude for fixed $\hat{k}$ and the projection of the potential onto a line defined by a unit vector $\hat{u}$. We consider a two-dimensional problem (the receivers are located on a curve and the velocity is a function of x and z). However, a three-dimensional formulation can be obtained following similar steps. Let

$$\hat{u} = \begin{bmatrix} \cos\varphi \\ \sin\varphi \end{bmatrix} \equiv \frac{\hat{k} - \hat{k}_s}{|\hat{k} - \hat{k}_s|} \tag{9a}$$

$$u \equiv k\ |\hat{k} - \hat{k}_s| = k\ 2\ |\hat{u} \cdot \hat{k}_s|\,, \tag{9b}$$

i.e., $\hat{u}$ is the unit vector along the direction $k-k_s$, and u is obtained by multiplying the wavenumber k by the length of $\hat{k}-\hat{k}_s$ as shown in Figure 2. The angle φ and the magnitude u can be simply related to the angles ϑ and ϑ_s as follows

$$\varphi = \frac{\vartheta + \vartheta_s \pm \pi}{2} \tag{10a}$$

$$u = k\ 2|\cos(\varphi-\vartheta_s)| = k\ 2|\sin(\frac{\vartheta-\vartheta_s}{2})| , \tag{10b}$$

where the sign of φ in equation (10a) is chosen such that $\vartheta_s + \pi/2 < \varphi < \vartheta_s + 3\pi/2$. Replacing the exponent $k-k_s$ in equation (8) by $u\hat{u}$, we find that for an angle ϑ which belongs to the angular aperture of the receiver array (i.e., $\vartheta \in [\ \alpha_2\ ;\ \alpha_1\ ]$) we have

$$A(\hat{k},\omega) = k^2\, S(\omega) \int_V dx'\, \gamma(x')\, e^{-iu\hat{u}\cdot x'} . \tag{11}$$

Thus, for fixed $\hat{k}$ and varying ω, the plane-wave scattering amplitude gives the Fourier transform of γ along a line with angle φ, where φ is algebraically related to the angle ϑ of $\hat{k}$ via equation (10a). If we consider all available plane-wave components we obtain a cone in the Fourier transform domain of γ, where the angles φ contained in this cone are given by

$$\varphi \in \Phi = \left[\ \frac{\alpha_2 + \vartheta_s \pm \pi}{2}\ ;\ \frac{\alpha_1 + \vartheta_s \pm \pi}{2}\ \right], \tag{12}$$

as shown in Figure 3. By taking the Fourier transform of both sides of equation (11) the projection of the potential onto the line defined by $\hat{u}$ is given by

$$\hat{\gamma}(\hat{u},s) = \int_V dx'\, \gamma(x')\, \delta(\ \hat{u}\cdot x' - s\ )$$

$$= \frac{1}{2\pi} \int_{-\infty}^{\infty} du\ \frac{A(\hat{k},\omega)}{k^2 S(\omega)}\, e^{ius} . \tag{13}$$

Finally, changing the integral variable from u to k according to equation (9b), we obtain

$$\hat{\gamma}(\hat{\underline{u}},s) = \frac{1}{\pi} |\hat{\underline{u}} \cdot \hat{\underline{k}}_s| \int_{-\infty}^{\infty} dk \; \frac{A(\hat{\underline{k}},\omega)}{k^2 S(\omega)} e^{ik2|\hat{\underline{u}} \cdot \hat{\underline{k}}_s|s} . \tag{14}$$

The projections of the velocity potential are given by equation (14) when $\hat{\underline{k}}$ is within the angular-aperture of the receiver array. The projections for the remaining angles cannot be obtained from the data. Therefore, if the receivers do not surround the medium, only a subset of the projections can be recovered. In this case, the reconstruction problem is similar to the limited angle tomography problem. The range of available projection angles is determined by the angles α_1, α_2 specifying the receiver array and by the angle ϑ_s of the incident plane wave (equation (12)). In the discussion above we have seen that for fixed $\hat{\underline{k}}$ and varying ω the plane-wave scattering amplitude gives the Fourier transform of γ along a line with angle φ. From the projection-slice theorem the inverse Fourier transform along this line gives the projection of the potential γ onto the line defined by the angle φ. This is the dual of the problem considered in diffraction tomography ([10]), where for fixed ω and varying $\hat{\underline{k}}$ the plane-wave scattering amplitude gives the Fourier transform of the potential along certain circular trajectories.

The velocity potential is reconstructed from its projections by Radon's inversion formula ([16])

$$\gamma(\underline{x}) = \frac{1}{2\pi} \int_{\Phi} d\hat{\underline{u}} \; \hat{\gamma}_f(\hat{\underline{u}}, \hat{\underline{u}} \cdot \underline{x}) , \tag{15}$$

where Φ is the range of available projections specified by equation (12), and where the filtered projections are defined as

$$\hat{\gamma}_f(\hat{\underline{u}},\rho) \equiv \frac{1}{2\pi} \int_{-\infty}^{\infty} du \; e^{iu\rho} |u| \int_{-\infty}^{\infty} ds \; e^{-ius} \hat{\gamma}(\hat{\underline{u}},s) . \tag{16}$$

From equations (9b) and (13), the filtered projections can be written in terms of the scattering amplitude as

$$\hat{\gamma}_f(\hat{\underline{u}},\rho) = \frac{2}{\pi} |\hat{\underline{u}} \cdot \hat{\underline{k}}_s|^2 \int_{-\infty}^{\infty} dk \; \frac{A(\hat{\underline{k}},\omega)}{|k| S(\omega)} e^{ik2|\hat{\underline{u}} \cdot \hat{\underline{k}}_s|\rho} . \tag{17}$$

For a given array geometry, the scattering amplitude obtained in equation (7) can be substituted in the above equation, thus providing a direct relation between the observed data and the projections of the potential.

From equation (7), we see that both the scattered field and its normal derivative are needed to obtain the plane-wave scattering amplitude. It is easy to show that for a straight-line receiver array the two terms inside the brackets in equation (7) become identical, so that only the scattered field itself is needed to obtain the scattering amplitude. In general the normal derivative of the scattered field along a curve (or surface) can be obtained from the field itself, but there is no simple analytical expression between these two quantities. In the next section we consider the case of a straight-line receiver array.

Straight-line receiver array

Consider the observation geometry shown in Figure 4, where receivers are located on a straight line defined by the unit vector $\hat{\underline{s}}$. In this case, the plane-wave scattering amplitude becomes

$$A(\hat{\underline{k}},\omega) = 2\,\hat{\underline{n}} \cdot \hat{\underline{k}} \int_{-\infty}^{\infty} ds \; ik \; P_s(s,\omega)\, e^{-i\underline{k} \cdot (\underline{r}_0 + s\hat{\underline{s}})} , \tag{18}$$

where $\hat{\underline{n}}$ is the unit vector pointing towards the scatterers and $\underline{r}_0$ is the origin of the receiver array indicated in Figure 4. From equations (17) and (18), the filtered projections of the potential can be expressed directly in terms of the observed scattered field as follows

$$\hat{\gamma}_f(\hat{u},\rho) = \frac{4}{\pi} |\hat{u}\cdot\hat{k}_s|^2 \hat{n}\cdot\hat{k}$$

$$\int_{-\infty}^{\infty} ds \int_{-\infty}^{\infty} dk\ i\ sgn(\omega)\ \frac{P_s(s,\omega)}{S(\omega)}\ e^{-ik[\hat{k}\cdot(r_0+s\hat{s})-2|\hat{u}\cdot\hat{k}_s|\rho]}, \qquad (19)$$

where $sgn(\omega)$ denotes the sign of ω. The expression inside the integral in equation (19) can be interpreted as obtained by the following sequence of steps :

1) First, we perform a deconvolution of $P_s(s,\omega)$, so that $P_s(s,\omega)$ is multiplied by $1/S(\omega)$.

2) The resulting deconvolved field is then Hilbert transformed, which corresponds to a multiplication by $isgn(\omega)$.

3) The dk integral corresponds to an inverse Fourier transform.

The filtered projections can therefore be expressed in the time domain as

$$\hat{\gamma}_f(\hat{u},\rho) = \frac{8}{c} |\hat{u}\cdot\hat{k}_s|^2 \hat{n}\cdot\hat{k}$$

$$\int_{-\infty}^{\infty} ds\ P_d^H(s,\ t = \frac{1}{c}\hat{k}\cdot r_0 - \frac{2}{c}|\hat{u}\cdot\hat{k}_s|\ \rho + \frac{1}{c}\hat{k}\cdot\hat{s}\ s), \qquad (20)$$

where $P_d^H(s,t)$ is the deconvolved and Hilbert transformed data and where the ds integral corresponds to a slant-stack operation.

Weak-curvature receiver array

If the receiver array is not a straight-line both the scattered field and its normal derivative are needed to obtain the projections. It can be seen from equations (7) and (17) that in this case the projections are obtained by slant-stacking both the field and its normal derivative. This increases the processing time by a factor of two. Moreover, if the normal derivative field is not observed, it must be obtained from the field observations numerically. However, if the local radius of curvature of the receiver array is much larger than the dominant wavelength, the normal derivative field can be approximately written in terms of the field along

the array. The simplest way is to assume that the receiver array is locally a straight line. With this assumption the plane-wave scattering amplitude becomes

$$A(\hat{\underline{k}},\omega) = 2 \int_{-\infty}^{\infty} ds\ \hat{\underline{n}}(s) \bullet \hat{\underline{k}}\ ik\ P_s(\underline{r},\omega)\ e^{-ik \bullet [\underline{r}_0 + s\hat{\underline{s}}(s)]} . \qquad (21)$$

This is essentially the same expression as in equation (18) except that the tangent ($\hat{\underline{s}}$) and normal ($\hat{\underline{n}}$) unit vectors are functions of the receiver location. Therefore, the filtered projections in this case are given by

$$\hat{\gamma}_f(\hat{\underline{u}},\rho) = \frac{8}{c} |\hat{\underline{u}} \bullet \hat{\underline{k}}_s|^2$$

$$\int_{-\infty}^{\infty} ds\ \hat{\underline{n}}(s) \bullet \hat{\underline{k}}\ P_d^H[s,\ t = \frac{1}{c}\hat{\underline{k}} \bullet \underline{r}_0 - \frac{2}{c} |\hat{\underline{u}} \bullet \hat{\underline{k}}_s|\ \rho + \frac{1}{c}\hat{\underline{k}} \bullet \hat{\underline{s}}(s)\ s] . \qquad (22)$$

For straight-line and weak-curvature receiver arrays, the slant-stacking reconstruction method consists therefore in obtaining first the filtered projections $\hat{\gamma}_f(\hat{\underline{u}},\rho)$ via equations (20) or (22), and then in using (15) to reconstruct the potential $\gamma(\underline{r})$.

3. Inversion by imaging-filtering

The second inversion method considered here consists of a sequence of steps where the scattered field is first backpropagated inside the medium, imaged at the travel times and then filtered in space. Consider the extrapolated wavefield $P_e(\underline{r},\omega)$ defined by

$$P_e^*(\underline{r},\omega) \equiv \int_R dl\ [\ P_s(\underline{r}_R,\omega)\ \nabla G_0^*(\underline{r},\underline{r}_R,\omega) -$$

$$\nabla P_s(\underline{r}_R,\omega)\ G_0^*(\underline{r},\underline{r}_R,\omega)\ ] \bullet \hat{\underline{n}} , \qquad (23)$$

where R denotes the curve where the receivers are located, $\hat{\underline{n}}$ is the normal unit

vector pointing towards the scatterers, and G_0^* is the complex conjugate of the Green's function. The extrapolated field P_e is the solution of a boundary value problem for the homogeneous wave operator, where the time reversed scattered field P_s^* and its normal derivative are imposed as boundary conditions at the receiver locations ([17]). In equation (23), due to the presence of the incoming Green's function G_0^*, the observed data is backpropagated towards the scatterers to obtain the extrapolated field. The backpropagated field converges and focuses (collapses) at the scatterers in the medium and then diverges and propagates away from the scatterers. Therefore, the extrapolated field contains both incoming and outgoing waves. The extrapolated field concept has been used in various problems previously. Porter [17] introduced the idea in the holographic imaging context to analyze the image kernels for various array geometries. Bojarski [18] used this concept to study the inverse source problem, and Esmersoy et. al. [12] used it for the inverse scattering problem for a single wide-band point source. Also, the mapping principle of migration for reflection data introduced by Claerbout [19] is essentially the travel time imaging of the extrapolated field.

The following volume integral representation of the extrapolated field can be obtained from equations (6) and (23)

$$P_e^*(\underline{r},\omega) = k^2\, S(\omega) \int_V d\underline{r}'\, \gamma(\underline{r}')\, e^{i\underline{k}_s \cdot \underline{r}'}\, E(\underline{r},\underline{r}',\omega)\,, \tag{24}$$

where the extrapolated field kernel is defined as

$$E(\underline{r},\underline{r}',\omega) \equiv \int_R d\underline{l}\ [\ G_0(\underline{r}_R,\underline{r}',\omega)\ \nabla G_0^*(\underline{r},\underline{r}_R,\omega) - \nabla G_0(\underline{r}_R,\underline{r}',\omega)\ G_0^*(\underline{r},\underline{r}_R,\omega)\ ] \cdot \hat{\underline{n}}\,. \tag{25}$$

The kernel appearing in equation (24) represents the contribution of the field scattered from point $\underline{r}'$ to the field extrapolated to $\underline{r}$. Comparing equations (6) and (24) $E(\underline{r},\underline{r}',\omega)$ can be interpreted as the "Green's function" for the extrapolated field. It was shown by Porter [18] that when R is an open surface asymptotic to a wedge of angular range $[\alpha_2\ ;\ \alpha_1]$, the extrapolated field kernel can be written as

$$E(\underline{r},\underline{r}',\omega) = \frac{i\,sgn(\omega)}{4\pi} \int_{\alpha_2}^{\alpha_1} d\vartheta\; e^{i\underline{k}\cdot(\underline{r}-\underline{r}')}\,, \tag{26}$$

where ϑ is the angle corresponding to the unit vector $\hat{\underline{k}}$ and $\underline{k} = k\hat{\underline{k}}$. Let now

$$\beta(\underline{r}) \equiv -\frac{1}{2\pi} \int_{-\infty}^{\infty} d\omega\; \frac{P_e^*(\underline{r},\omega)}{i\omega\, S(\omega)}\, e^{-i\underline{k}_s\cdot\underline{r}}\,, \tag{27}$$

be the function obtained by filtering the extrapolated field, and by imaging it at the source travel times $\tau(\underline{r}) = \frac{1}{c}\hat{\underline{k}}_s \cdot \underline{r}$ (which corresponds to a plane-wave source and a homogeneous background). Here the filter $[i\omega S(\omega)]^{-1}$ corresponds to a deconvolution operation followed by an integration in the time domain. From equation (23) it is seen that the filtered extrapolated field can be obtained by first filtering the scattered field and then backpropagating the resulting field into the medium. The travel time image $\beta(\underline{r})$ is similar to the migrated image except for the time integration performed before extrapolation. It turns out that $\beta(\underline{r})$ is simply a spatially filtered version of the velocity potential $\gamma(\underline{r})$ where the filter impulse response depends on the incidence angle of the plane wave and the angle-aperture of the receiver array. To see this, combine equations (24), (26) and (27). Then, the travel time image can be expressed as

$$\beta(\underline{r}) = \int_V d\underline{r}'\, \gamma(\underline{r}')\, h(\underline{r}-\underline{r}')\,, \tag{28}$$

where $h(\bullet)$ is a space-invariant filter with point spread function

$$h(\underline{r}) = -\frac{1}{8\pi^2} \int_{\alpha_2}^{\alpha_1} d\vartheta \int_{-\infty}^{\infty} dk\;\; |k|\; e^{ik(\hat{\underline{k}}-\hat{\underline{k}}_s)\cdot\underline{r}}\,. \tag{29}$$

Thus, the image $\beta(\underline{r})$ represents the velocity potential filtered by the space-invariant filter given above. This filter has a simple interpretation in the Fourier domain. Consider the change of variables given by equations (9a) and (9b) and

let φ be the angle corresponding to the unit vector $\hat{u}$. In terms of the new coordinates $(\varphi\ ,\ u)$ the filter can be written as

$$h(\underline{r}) = -\frac{1}{16\pi^2} \int_{\Phi} \frac{d\varphi}{|\hat{u} \bullet \hat{k}_s|^2} \int_{-\infty}^{\infty} du\ |u|\ e^{iu\hat{u} \bullet \underline{r}}\ , \tag{30}$$

where Φ is the integration range for the angles φ corresponding to $\vartheta \in [\alpha_2\ ;\ \alpha_1]$. Define an extended range of angles Θ such that if $\varphi \in \Phi$ then both φ and $\varphi + \pi \in \Theta$. Then, equation (30) can be written as

$$h(\underline{r}) = -\frac{1}{4\pi^2} \int_{\Theta} d\varphi \int_{0}^{\infty} du\ u\ e^{iu\hat{u} \bullet \underline{r}}\ \frac{1}{4|\hat{u} \bullet \hat{k}_s|^2}\ ,$$

$$= \mathbf{FT}^{-1} \left\{ -\frac{N_\Theta}{4|\hat{u} \bullet \hat{k}_s|^2} \right\}, \tag{31}$$

where $\mathbf{FT}^{-1}$ denotes the multidimensional inverse Fourier transform and

$$N_\Theta = 1 \quad ; \quad \varphi \in \Theta$$

$$= 0 \quad ; \quad \text{otherwise}\ . \tag{32}$$

The Fourier magnitude of the filter $h(\underline{r})$ for the case of a line array and when the plane wave is at normal incidence is shown in Figure 5. From equation (28), we see that the potential $\gamma(\underline{r})$ can be obtained by deconvolving the image $\beta(\underline{r})$ with the filter $h(\underline{r})$. However, in general the inverse filter does not exist because of the zero region of N_Θ in the Fourier transform of $h(\underline{r})$. This zero region is determined by the array geometry and the incidence angle of the plane wave. It can be shown that, in fact, the zero region N_Θ corresponds to the missing projections of the potential discussed in Section 2. Since we cannot deconvolve in this region, the Fourier transform of γ cannot be recovered in the domain where N_Θ is zero. Although other choices could be made, we set the Fourier transform of γ to zero in this region. This corresponds to setting the missing projections to zero in the slant-stack method. A partial reconstruction $\gamma_{REC}(\underline{r})$ of the potential is

then given by

$$\gamma_{REC}(\underline{x}) = \mathbf{FT}^{-1}\left\{ -4\,|\,\hat{\underline{u}} \bullet \hat{\underline{k}}_s\,|^2\,\tilde{\beta}(u\hat{\underline{u}}) \right\}, \tag{33}$$

where $\tilde{\beta}(\underline{u})$ is the spatial Fourier transform of $\beta(\underline{x})$.

The imaging-filtering method can be summarized as follows. First, the observed scattered field is deconvolved by the source wavelet, integrated in time and backpropagated into the medium. The backpropagation can be done by using the Kirchhoff integral in equation (23). Note that, except for the straight-line array case, both the field and its normal derivative are required in the Kirchhoff integral. An alternative way to obtain the extrapolated field is to implement the boundary value problem specifying this field by the finite-difference method. In this approach the observations of the field alone are sufficient to obtain the extrapolated field. This is accomplished by running the finite-difference algorithm without any sources, and by using the time-reversed scattered field to specify the boundary values at the receiver locations. The second step of the imaging-filtering method is to image the extrapolated field at every point in the medium at the corresponding travel time of the incident source field. For the homogeneous background problem, considered here, the travel times can be computed analytically. In the third and final step, using equation (27), the resulting travel time image is filtered by the approximate inverse filter of the point spread function.

4. Examples

In this section we give some examples for the slant-stack and imaging-filtering methods discussed in the previous sections. We consider a two dimensional medium in which velocities do not vary along the y-axis. The data used in the examples are obtained by a finite difference algorithm. In all cases a four point Blackman window with approximately 50 Hz bandwidth (corresponds to a pulse duration of 0.02 seconds) is used as the source wavelet. The synthetic traces are deconvolved, using a Wiener inverse filter, before further processing.

The velocity structure and the observation geometry of the first example is shown in Figure 6(a). In this example the scatterer is a high velocity cylindrical object (the figure shows the cross-section in the plane $y = 0$) with a 14 meter diameter, which is approximately equal to the smallest wavelength contained in the exciting wavelet. The medium is probed by a normally incident plane wave and the scattered field is recorded on the surface ($z = 0$) along a 128 meter horizontal array, and along a 64 meter vertical array. The scattered field is shown in Figure 6(b) where h and v indicate the horizontal and vertical arrays respectively. The projections of the velocity potential are shown in Figure 7. Note that by simply using appropriate phase shifts on the data we can choose any point in the medium as the origin for the projections. Here we choose the center of the scatterer ($x = 64$, $z = 18$) as the origin to display the projections. The true projections obtained from the velocity model used to create the synthetics are shown in Figure 7(a). Since the object is circularly symmetric, the projections at all angles are the same. Figure 7(b) shows the projections obtained from the scattered field observed along the horizontal receiver array only. Figure 7(c) describes the projections recovered from the horizontal array combined with the vertical array. From equation (12), for an infinite horizontal array ($\alpha_2 = 180°$, $\alpha_1 = 360°$) the range of available projections is $225° < \varphi < 315°$ and for an infinite horizontal-vertical array ($\alpha_2 = 180°$, $\alpha_1 = 450°$) the range is given by $225° < \varphi < 360°$. For finite length arrays, however, only a subset of these projections can be recovered as can be seen from Figures 7(b,c). The slant-stack inversion result is shown in Figure 8 for the region indicated in Figure 6(a) by dashed lines. Figures 8(a) and 8(b) are the results obtained by using only the horizontal

array, and the combined horizontal and vertical arrays, respectively. Figures 9(a) and 9(b) show the velocity structure obtained by the imaging-filtering method for the same data sets. It is seen that the two methods give very similar results.

In the second example, shown in Figure 10, the scattering medium consists of two halves of a cylinder. The velocities in the top and bottom halves are lower and higher than the background velocity, respectively. The velocity contrast between the two regions is about 14% and the radius of the cylinder is 15 meters, approximately one minimum wavelength. The medium is probed by a plane wave with angle of incidence $\vartheta_s = 45°$, and the scattered field is observed on the surface and along two vertical arrays on both sides of the object. The length of each line array is about ten minimum wavelengths or five times the size of the scatterer. The scattered fields observed along the vertical array located at offset $x = 0$, on the surface, and along the vertical array located at offset $x = 150$ meters are shown in Figures 11(a), (b) and (c), respectively. The projections of the velocity potential are shown in Figure 12, where the projection origin is chosen at $x = z = 75$ meters. The true projections obtained from the velocity model are shown in Figure 12(a), where the shaded region corresponds to the positive values of γ, i.e. velocities lower than the background velocity. Figures 12(b), (c) and (d) are the projections obtained from the observed data. Figure 12(b) is obtained by using the surface array only, (c) by using the surface array combined with the vertical array at zero offset and (d) illustrates the result obtained by using all three arrays. Note that the projections in the range of angles 135° to 315° represent a complete set from which the potential can be totally reconstructed. However, due to the finite extent of the arrays and the fact that the data is bandlimited , we can recover only a portion of the projections with this experiment. In general, the missing projections can be obtained by performing several experiments with appropriately chosen probing waves. For example, for the receiver geometry used in this example, a second probing wave with an angle of incidence equal to 135° could provide the proper complementary coverage. Figure 13 shows the inversion results using all three receiver arrays. Figure 13(a) is the result of the slant-stack method. Figure 13(b) shows the travel time image $\beta(\underline{x})$ (defined by equation (27)), and Figure 13(c) is the result obtained by filtering $\beta(\underline{x})$ via equation (33). Figure 13(d) shows the inversion result for the case

where a second probing wave with an angle of incidence equal to 135° is used to obtain a complementary coverage.

5. Conclusion

In this paper we have considered the direct velocity inversion problem for a constant density acoustic medium probed by a single wide-band plane wave. Two methods, namely, the slant-stack and imaging-filtering methods, have been presented for partially reconstructing the velocities of the medium from the observed scattered field. It was shown that there is a simple map between the plane-wave components of the scattered field, which are obtained by performing slant-stack operations on the observed data, and the projections of the velocity potential of the medium. The range of plane-wave components and the range of angles of projections that can be recovered from the observed data is determined by the aperture of the receiver array. In the slant-stack method, first the projections of the potential are obtained from the plane-wave scattering amplitudes. Then, the medium velocities are reconstructed partially from the available projections via well-known methods of tomography and by setting the unknown projections to zero. The imaging-filtering method consists of two-steps. First, the observed data is filtered in time, backpropagated into the medium and imaged at the travel times, as in migration. It is shown that the resulting travel time image is simply a spatially filtered version of the velocity potential. The filter relating the two is space-invariant, and is completely determined by the angle of incidence of the probing plane wave and by the aperture of the receiver array. Therefore, in the second step, the velocities of the medium can be obtained by filtering the travel time image with an inverse filter designed for the given experiment geometry. It is seen that, if the receivers do not surround the medium (incomplete coverage), the exact inverse filter does not exist and the velocities can only be obtained approximately.

An interesting extension of the results discussed in this paper would be to analyze the case where, instead of using a single plane-wave source, several plane waves are used to probe the scattering medium. Indeed, as was noted in the second example of Section 4, the use of several plane waves improves

considerably the resolution of the reconstructed image of the velocity potential. For the slant-stacking reconstruction method, the use of several plane waves requires some averaging of the projections obtained for each experiment. Another extension that we are currently investigating is for the case of a single point source. Note that the case when the receivers provide a complete coverage was examined in [12], but the incomplete receiver coverage case is more complicated, and may require the use of a space-variant filter instead of the space-invariant filter employed in the imaging-filtering method described above.

---

a)The work of this author was supported by the Army Research Office under Grant No. DAAG29-84-K-0005, and by the National Science Foundation under Grant ECS-83-12921.

Appendix A : Derivation of the Relation Between Plane-Wave Components of the Scattered Field and Projections of the Velocity Potential

In this appendix the relation (8) between the plane-wave scattering amplitude and the velocity scattering potential is derived for an arbitrary receiver array with angular-aperture $[\ \alpha_2\ ;\ \alpha_1\ ]$ as shown in Figure A1. The plane-wave scattering amplitude is defined as

$$A(\hat{\underline{k}},\omega) = -\int_R dl\ [\ P_s(\underline{r},\omega)\ \nabla e^{-i\underline{k}\cdot\underline{r}} - \nabla\ P_s(\underline{r},\omega)\ e^{-i\underline{k}\cdot\underline{r}}\ ]\cdot\hat{\underline{n}}\ , \qquad \text{(A1)}$$

where R is the surface where the receivers are located and $\hat{\underline{n}}$ is the unit normal vector pointing towards the scatterers as in Figure A1. From equations (6) and (A1) we have

$$A(\hat{\underline{k}},\omega) = k^2\ S(\omega) \int_V d\underline{r}'\ \gamma(\underline{r}')\ e^{i\underline{k}_s\cdot\underline{r}'}\ I(\underline{k},\underline{r}')\ , \qquad \text{(A2)}$$

$$I(\underline{k},\underline{r}') \equiv -\int_R d\underline{r}\ [\ G_0(\underline{r},\underline{r}',\omega)\ \nabla e^{-i\underline{k}\cdot\underline{r}} - \nabla\ G_0(\underline{r},\underline{r}',\omega)\ e^{-i\underline{k}\cdot\underline{r}}\ ]\cdot\hat{\underline{n}}\ . \qquad \text{(A3)}$$

Here, $G_0(\underline{r},\underline{r}',\omega)$ is the free space Green's function, and as indicated in (5a), in two-dimensions it is given by

$$G_0(\underline{r},\underline{r}',\omega) = \frac{i}{4}\ H_0^{(1)}(k\ |\underline{r}-\underline{r}'|)\ . \qquad \text{(A4)}$$

Now, consider the arc S of the circle of infinite radius centered at $\underline{r}'$ which is shown in Figure A1. Since there are no scatterers within the volume surrounded by the closed surface $R+S$, from Green's theorem we have

$$I(\underline{k},\underline{r}') \equiv \int_S d\underline{r}\ [\ \frac{i}{4}H_0^{(1)}(k\ |\underline{r}-\underline{r}'|)\ \nabla e^{-i\underline{k}\cdot\underline{r}} - \nabla\ \frac{i}{4}H_0^{(1)}(k\ |\underline{r}-\underline{r}'|)\ e^{-i\underline{k}\cdot\underline{r}}\ ]\cdot\hat{\underline{n}}\ . \qquad \text{(A5)}$$

Let (r,ψ) be the polar coordinates centered at x' and let ϑ be the angle corresponding to the unit vector $\hat{k}$. Then, in this coordinate system the boundary integral in equation (A5) takes the form

$$I(k,x') = e^{-ik\cdot x'} \lim_{r\to\infty} r \int_{\alpha_2}^{\alpha_1} d\psi \left[\frac{i}{4} H_0^{(1)}(kr) \frac{\partial}{\partial r} e^{-ikr\cos(\psi-\vartheta)} - \right.$$

$$\left. \frac{\partial}{\partial r} \frac{i}{4} H_0^{(1)}(kr)\, e^{-ikr\cos(\psi-\vartheta)} \right] . \qquad \text{(A6)}$$

For $r \to \infty$ and $k \neq 0$, we have the following asymptotic expansion of the Green's function and its normal derivative

$$\lim_{r\to\infty} \frac{i}{4} H_0^{(1)}(kr) = \lim_{r\to\infty} \frac{e^{i\frac{\pi}{4}sgn(\omega)}}{(8\pi)^{1/2}} \frac{e^{ikr}}{|k|^{1/2} r^{1/2}} , \qquad \text{(A7)}$$

$$\lim_{r\to\infty} \frac{\partial}{\partial r} \frac{i}{4} H_0^{(1)}(kr) = \lim_{r\to\infty} ik \frac{i}{4} H_0^{(1)}(kr) . \qquad \text{(A8)}$$

Consequently, as $r \to \infty$, the boundary integral becomes

$$I(k,x') = -e^{-ik\cdot x'} \lim_{r\to\infty} \frac{i}{4} H_0^{(1)}(kr)\, ikr$$

$$\int_{\alpha_2}^{\alpha_1} d\psi \left[\cos(\psi - \vartheta) + 1 \right] e^{-ikr\cos(\psi-\vartheta)} . \qquad \text{(A9)}$$

The above integral can be evaluated by the method of stationary phase. The stationary points ψ_0 of the phase function are given by

$$\frac{\partial}{\partial \psi} k\cos(\psi - \vartheta) \Big|_{\psi=\psi_0} = 0 , \qquad \text{(A10)}$$

so that $\psi_0 = \vartheta$, $\vartheta+\pi$. For $\psi_0 = \vartheta + \pi$ the integrand of equation (A9) vanishes, therefore the only stationary point to be considered is $\psi_0 = \vartheta$. Now, if ϑ is not

within the integration range $[\alpha_2 ; \alpha_1]$, there is no contribution from this point and the integral is zero. However, if $\vartheta \in [\alpha_2 ; \alpha_1]$ equation (A9) becomes

$$I(\underline{k},\underline{r}') = -e^{-i\underline{k}\cdot\underline{r}'} \lim_{r\to\infty} \frac{i}{4} H_0^{(1)}(kr)\, ikr\; e^{i\frac{\pi}{4}sgn(\omega)} \left|\frac{2\pi}{kr}\right|^{\frac{1}{2}} 2e^{-ikr} \; . \tag{A11}$$

Finally, using the asymptotic form of the Green's function given in equation (A7), and noting that

$$ikr\; e^{i\frac{\pi}{2}sgn(\omega)} = -|kr| \; , \tag{A12}$$

we obtain

$$\begin{aligned} I(\underline{k},\underline{r}') &= e^{i\underline{k}\cdot\underline{r}'} \quad ; \quad \vartheta \in [\alpha_2 ; \alpha_1] \\ &= 0 \quad ; \quad \text{otherwise} \; . \end{aligned} \tag{A13}$$

Using this expression in equation (A2), we find that the plane-wave scattering amplitude is given by

$$\begin{aligned} A(\hat{\underline{k}},\omega) &= k^2\, S(\omega) \int_V d\underline{r}'\, \gamma(\underline{r}')\, e^{-i(\underline{k}-\underline{k}_0)\cdot\underline{r}'} \quad ; \quad \vartheta \in [\, \alpha_2 ; \alpha_1 \,] \\ &= 0 \quad ; \quad \text{otherwise} \; . \end{aligned} \tag{A14}$$

References

[1] Taylor, J. R., *Scattering Theory* ,John-Wiley & Sons, Inc., 1972.

[2] Berkhout, A. J.,"Wavefield extrapolation techniques in seismic migration, a tutorial," *Geophysics* , Vol. 46, No. 12, pp. 1638-1656, December 1981.

[3] Cohen, J. K. and Bleistein, N.,"Velocity inversion procedure for acoustic waves," *Geophysics* , Vol. 44, No. 6, pp. 1077-1087, June 1979.

[4] Norton, S. J. and Linzer, M.,"Ultrasonic reflectivity imaging in three dimensions: Exact inverse scattering solutions for plane, cylindrical, and spherical apertures," *IEEE Trans. Biomedical Eng.* , BME-28, pp. 202-220, 1981.

[5] Raz, S.,"Three-dimensional velocity profile inversion from finite-offset scattering data," *Geophysics* , Vol. 46, No. 6, pp. 837-842, June 1981.

[6] Clayton, R. W. and Stolt, R. H.,"A Born-WKBJ inversion method for acoustic reflection data," *Geophysics* , Vol. 46, No. 11, pp. 1559-1567, November 1981.

[7] Wolf, E.,"Three-dimensional structure determination of semi-transparent objects from holographic data," *Optics Communications* , Vol. 1, pp. 153-156, 1969.

[8] Mueller, R. K., Kaveh, M. and Wade G.,"Reconstructive tomography and applications to ultrasonics," *Proc. IEEE* , Vol. 67, No. 4, pp. 567-587, April 1979.

[9] Greenleaf, J. K.,"Computerized tomography with ultrasound," *Proc. IEEE* , Vol. 71, No. 3, pp. 330-337, March 1983.

[10] Devaney, A. J.,"Geophysical diffraction tomography," *IEEE Trans. Geosience and Remote Sensing* , Vol. GE-22, No. 1, pp. 3-13, January 1984.

[11] Devaney, A. J. and Beylkin, G."Diffraction tomography using arbitrary source-receiver surfaces," *Ultrasonic Imaging* , Vol. 6, pp. 181-193, 1984.

[12] Esmersoy, C., Oristaglio, M. L. and Levy, B. C.,"Multidimensional Born velocity inversion: Single wide-band point source," *J. Acoust. Soc. Am.* , Vol. 78, No. 3, pp. 1052-1057, September 1985.

[13] Temme, P.,"A comparison of common-midpoint, single-shot and plane wave depth migration," *Geophysics* , Vol. 49, No. 11, pp. 1896-1907, November 1984.

[14] Weglein, A. B.,"Multidimensional seismic analysis: migration and inversion,"

Geoexploration , 20, pp. 47-60, 1982.

[15] Cheng, G. and Coen, S.,"The relationship between Born inversion and migration for common-midpoint stacked data," *Geophysics* , Vol. 49, No. 12, pp. 2117-2131, December 1984.

[16] Dudgeon, D. E. and Mersereau, R. M., *Multidimensional digital signal processing* , Prentice-Hall, Inc., New Jersey, 1984.

[17] Morse, P. M. and Feshbach H., *Methods of Theoretical Physics, Part I* , McGraw-Hill, 1953.

[18] Porter, R. P.,"Diffraction Limited, Scalar Image Formation with Holograms of Arbitrary Shape," *Journal of the Optical Society of America* , Vol. 60, No. 8, pp. 1051-1059, August 1970.

[19] Bojarski, N. N.,"A Survey of the Near-Field Far-Field Inverse Scattering Inverse Source Integral Equation," *IEEE Trans. Antennas and Propagation* , Vol. AP-30, No. 5, pp. 975-979, September 1982.

[20] Claerbout, J. F.,"Toward a Unified Theory of Reflector Mapping," *Geophysics* , Vol. 36, No. 3, pp. 467-481, 1971.

Figure Captions

Figure 1. Scattering experiment. The medium is probed by a wide-band plane wave and the scattered field is observed along a receiver array asymptotic to angles α_1 and α_2.

Figure 2. The relation between the angle of incidence ϑ_s of the plane-wave source, the angle ϑ of the scattered plane wave and the projection angle φ.

Figure 3. Coverage in the Fourier transform domain of the potential γ.

Figure 4. Straight-line receiver array; $\hat{\underline{s}}$ is the unit vector along the array, $\hat{\underline{n}}$ the normal unit vector pointing towards the scatterers, $\underline{x}_0$ an arbitrary origin along the array.

Figure 5. Fourier domain representation of the filter relating the migrated image to the velocity potential. The filter which is shown corresponds to the experiment where the receiver array is on the surface (x-axis) and the probing plane-wave is normally incident ($\vartheta_s = \pi/2$). (a) Zero and nonzero regions in the Fourier domain. (b) Fourier magnitude of the filter along the semi-circle shown in (a).

Figure 6. Scattering experiment. (a) High velocity cylindrical object probed by a normally incident plane wave. (b) Observed scattered field. The horizontal array on the surface is indicated by "h" and the vertical array is indicated by "v".

Figure 7. Projections $\hat{\gamma}(\hat{\underline{u}},s)$ of the velocity potential. The origin for the projections is chosen at the center of the object. The horizontal axis is the projection angle φ corresponding to the unit vector $\hat{\underline{u}}$, where the angle is measured clockwise from the x-axis. The vertical axis is the variable s. (a) True projections. (b) Projections obtained from the surface array only. (c) Projections recovered from the combined horizontal and vertical arrays.

Figure 8. The slant-stack inversion result for the region shown inside the dashed lines in Figure 6(a). One trace spacing corresponds to a $100\ m/s$ velocity difference from the background. Reconstruction (a) using only surface data, (b) using the combined surface and vertical data.

Figure 9. The imaging-filtering inversion result for the same region as in Figure 8. One trace spacing corresponds to $100m/s$ velocity difference from the background. Reconstruction (a) using surface data only, (b) using both surface and vertical data.

Figure 10. Scattering experiment. The medium is probed by a plane wave with 45° angle of incidence. The scattered field is observed on the surface and along two vertical arrays on both sides of the scatterer.

Figure 11. Observed scattered field in the time window 0.2–0.35 seconds. (a) The vertical array at zero offset (amplitude scale 0.1). (b) The surface array (scale 0.24). (c) The vertical array at offset 150 meters (scale 0.71).

Figure 12. Projections $\hat{\gamma}(\hat{\underline{x}},s)$ of the velocity potential. The origin for the projections is at $x = z = 75$ meters. The horizontal axis is the projection angle φ measured clockwise from the x-axis. The vertical axis is the variable s. (a) True projections. (b) Projections obtained from the surface array only. (c) Projections obtained from the surface array combined with the vertical array at zero offset. (d) Projections recovered from all three arrays.

Figure 13. Reconstruction. One trace spacing corresponds to a 50 m/s velocity difference from the background. (a) Slant-stack inversion result. (b) Travel time image $\beta(\underline{x})$. (c) The result obtained by filtering $\beta(\underline{x})$ in the imaging-filtering method. (d) Slant-stack inversion result for two probing plane waves with angles of incidence 45° and 135°.

Figure A1. Receiver array with angular aperture $[\alpha_2;\alpha_1]$. R is the curve where the receivers are located and S is the arc of the circle of infinite radius centered at $\underline{x}'$.

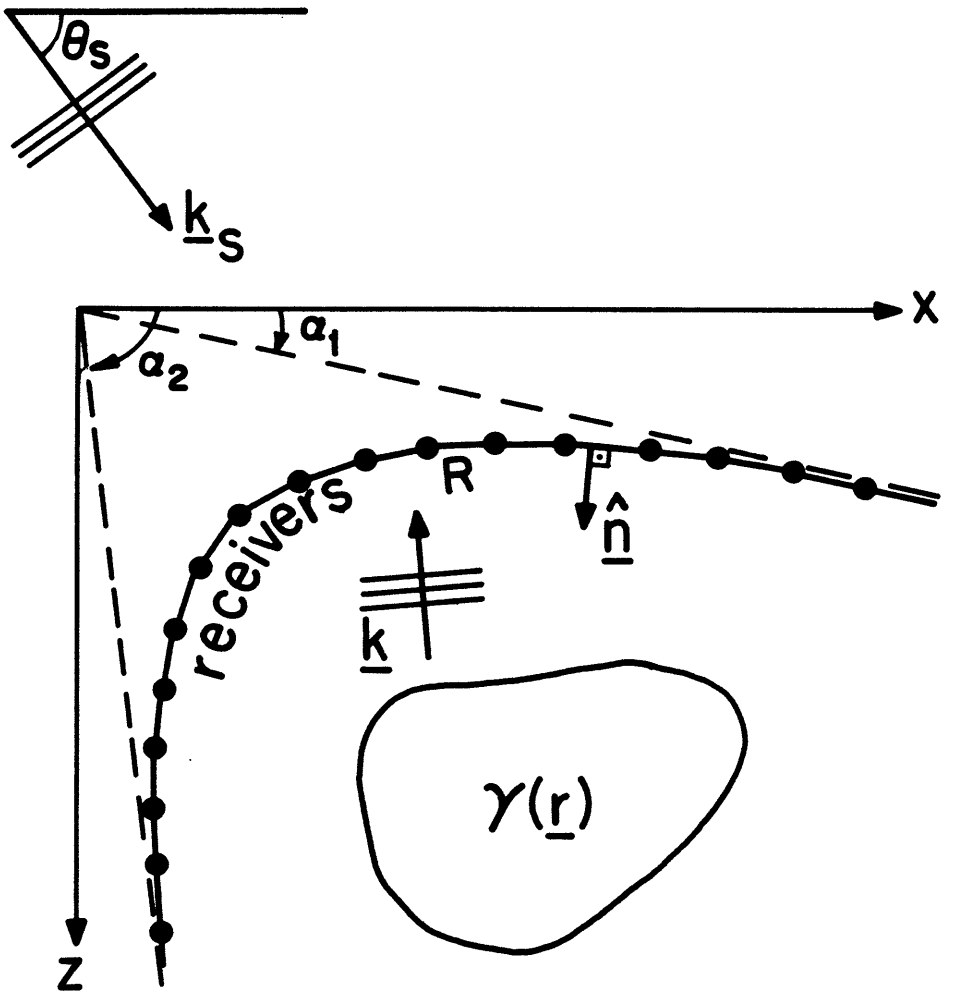

Figure 1

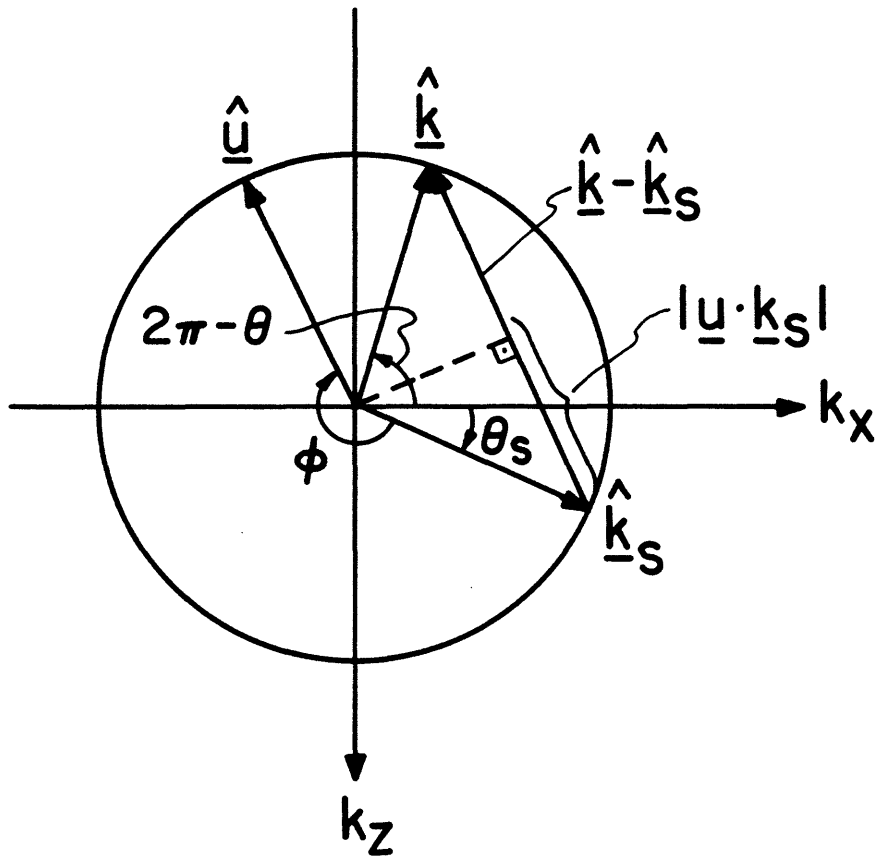
$\hat{u}$
$\hat{k}$
$\hat{k}-\hat{k}_s$
$2\pi-\theta$
$|u\cdot k_s|$
k_x
ϕ
θ_s
$\hat{k}_s$
k_z

Figure 2

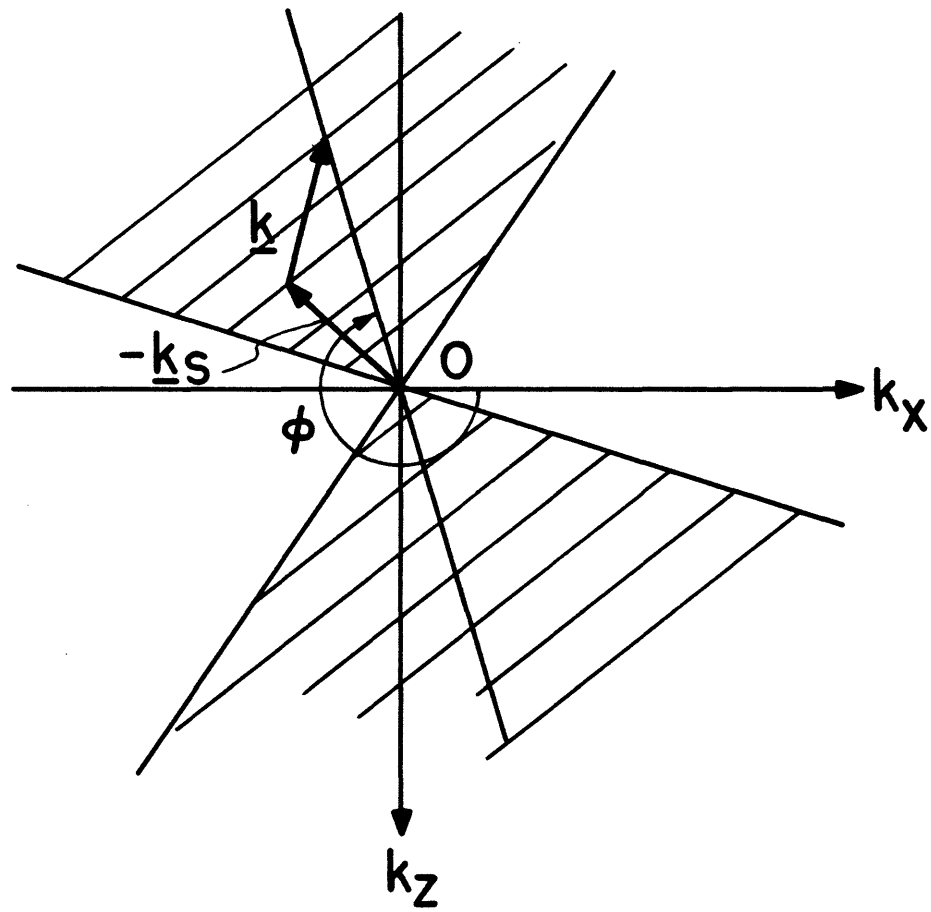

Figure 3

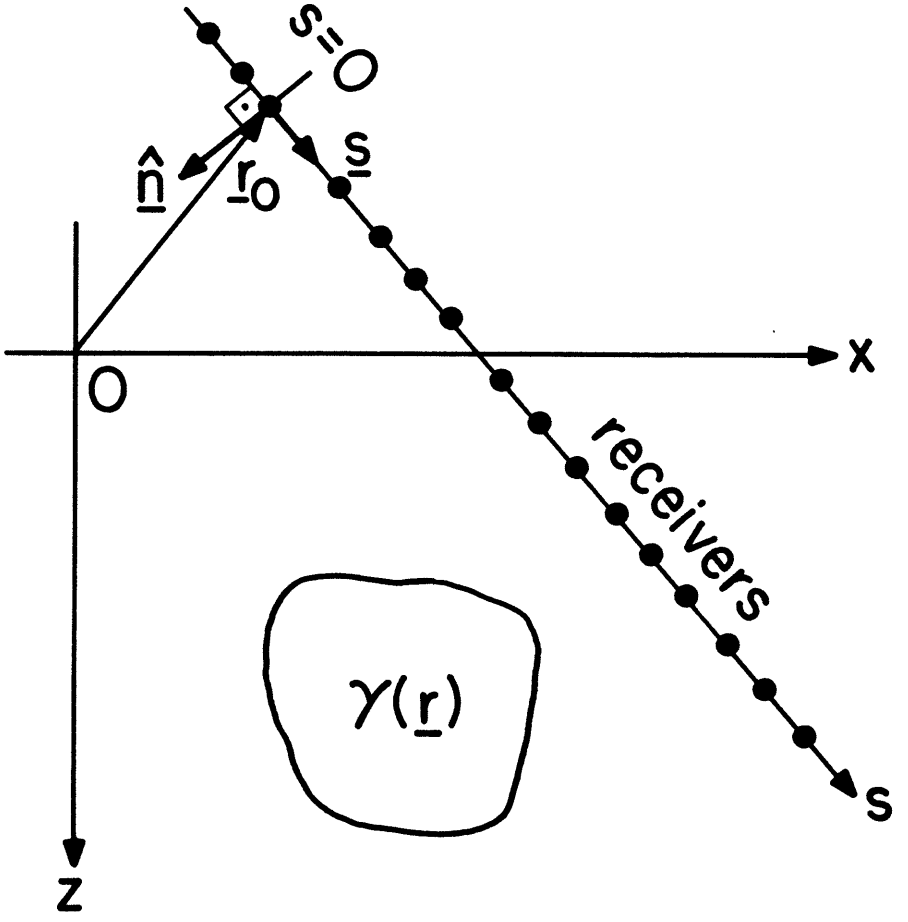

Figure 4

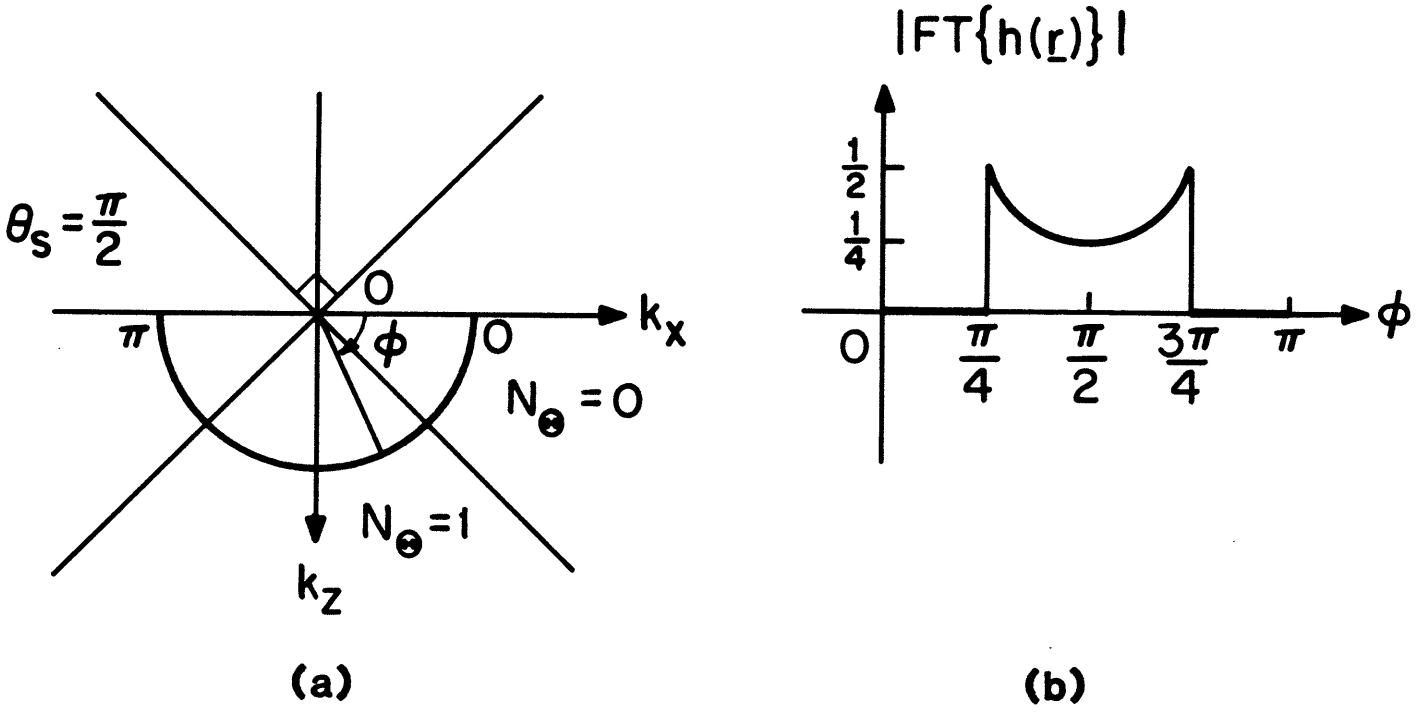
$\theta_s = \frac{\pi}{2}$
0
k_x
π
ϕ
0
$N_\Theta = 0$
$N_\Theta = 1$
k_z
(a)
$|FT\{h(\underline{r})\}|$
$\frac{1}{2}$
$\frac{1}{4}$
0
$\frac{\pi}{4}$
$\frac{\pi}{2}$
$\frac{3\pi}{4}$
π
ϕ
(b)

Figure 5

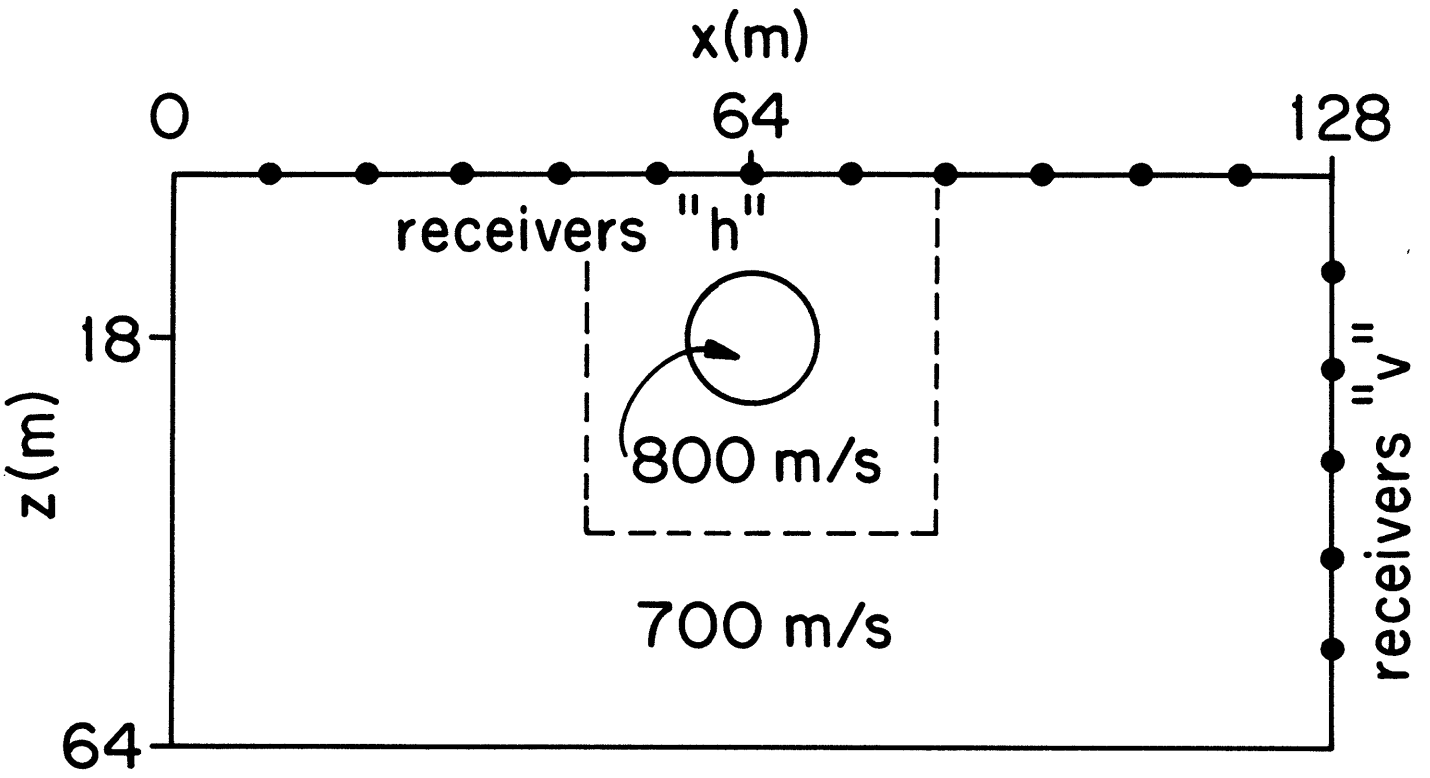

(a)

Figure 6

(b)

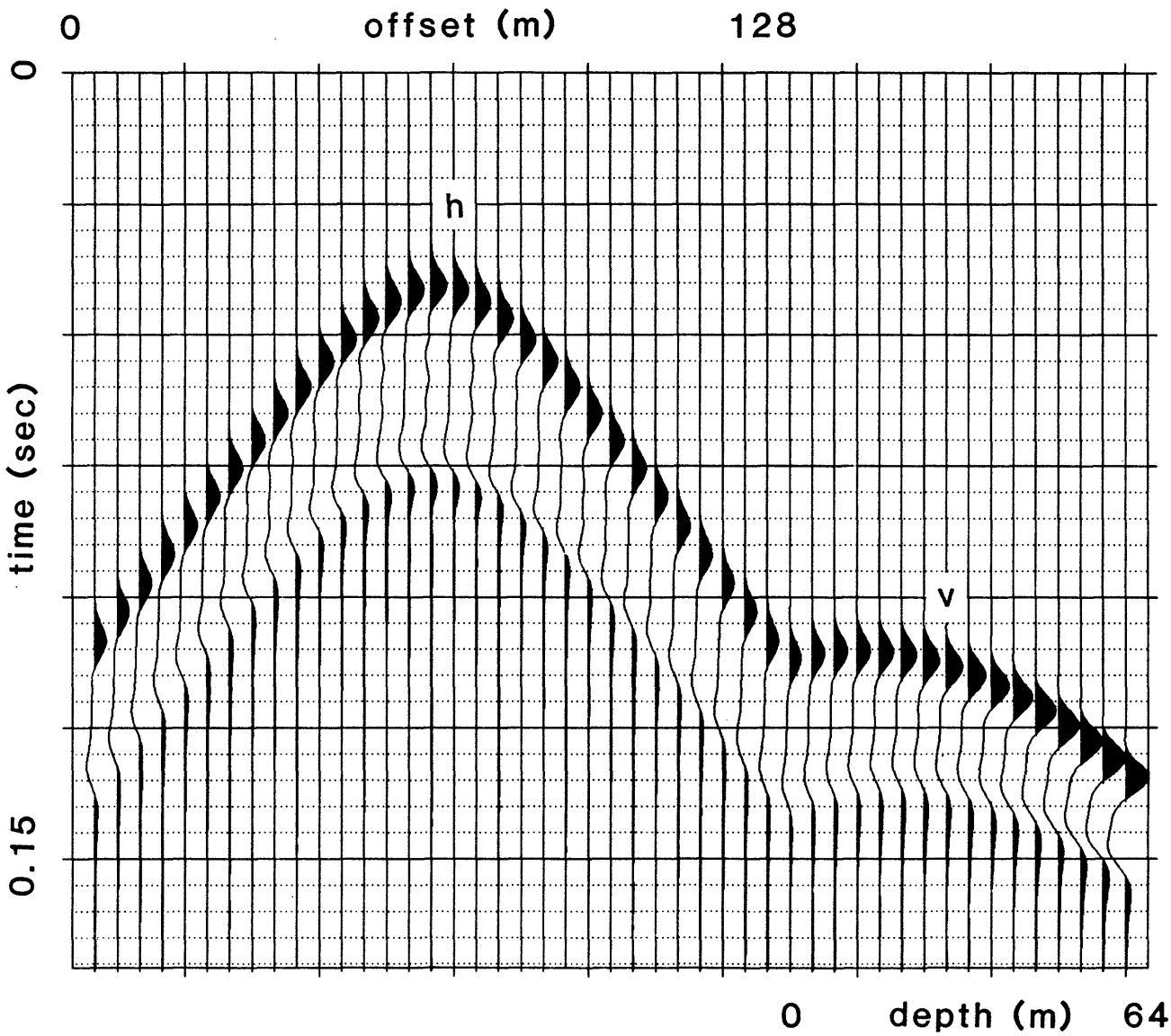

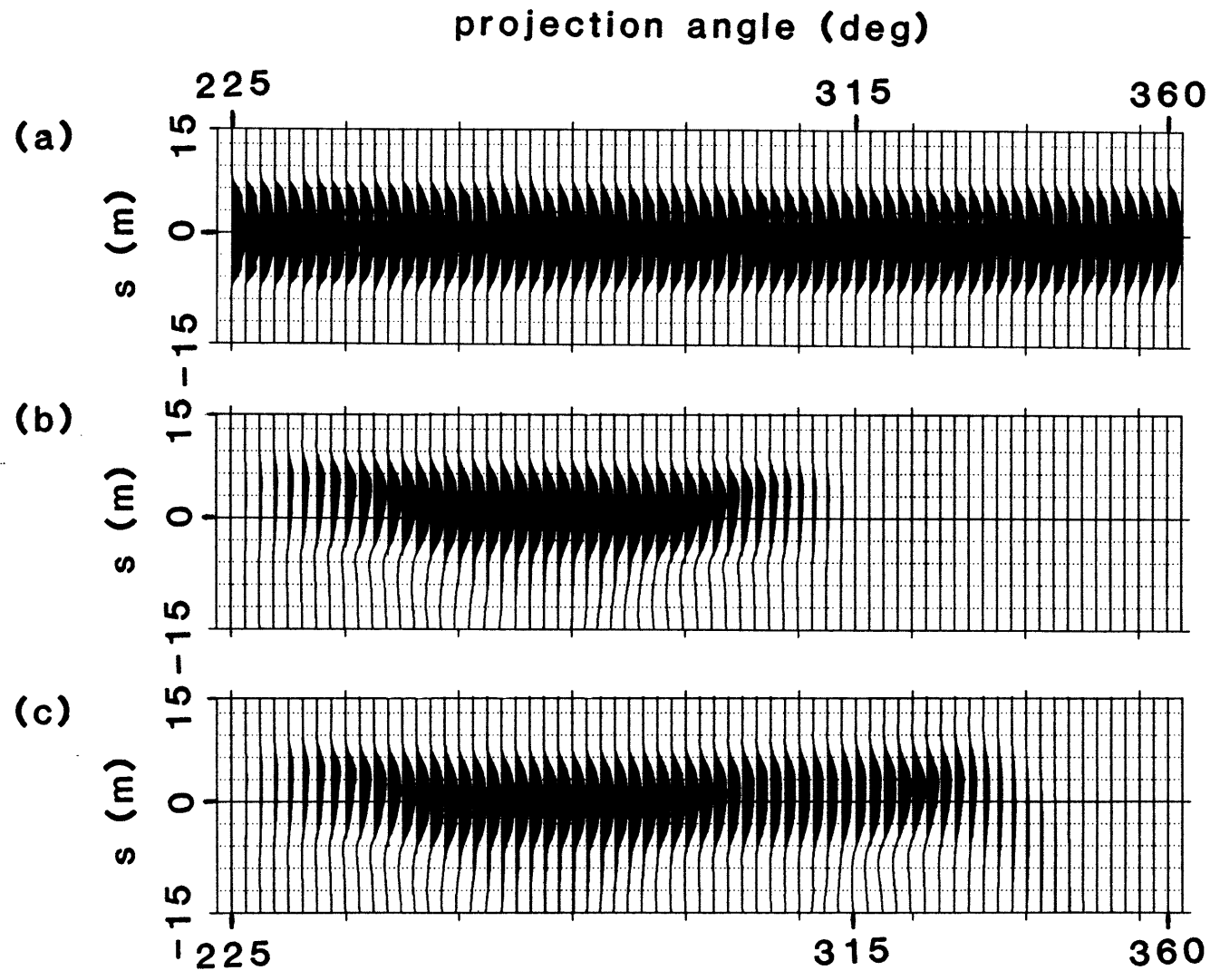

Figure 7

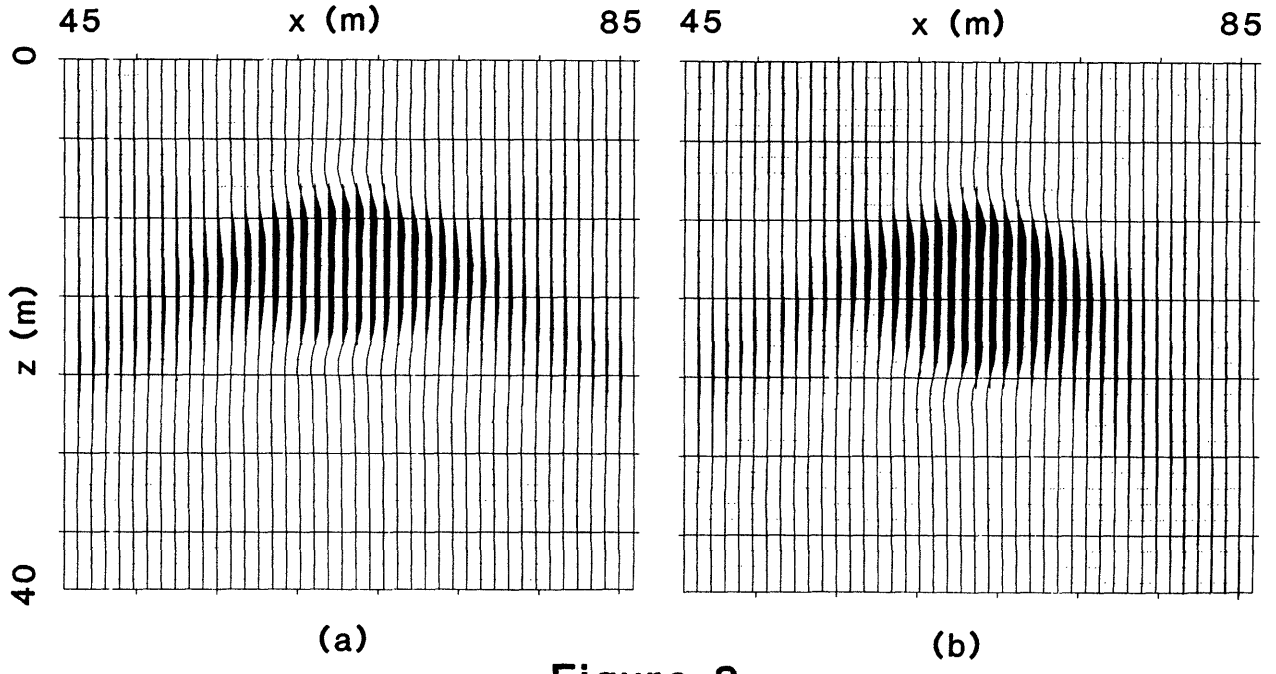

Figure 8

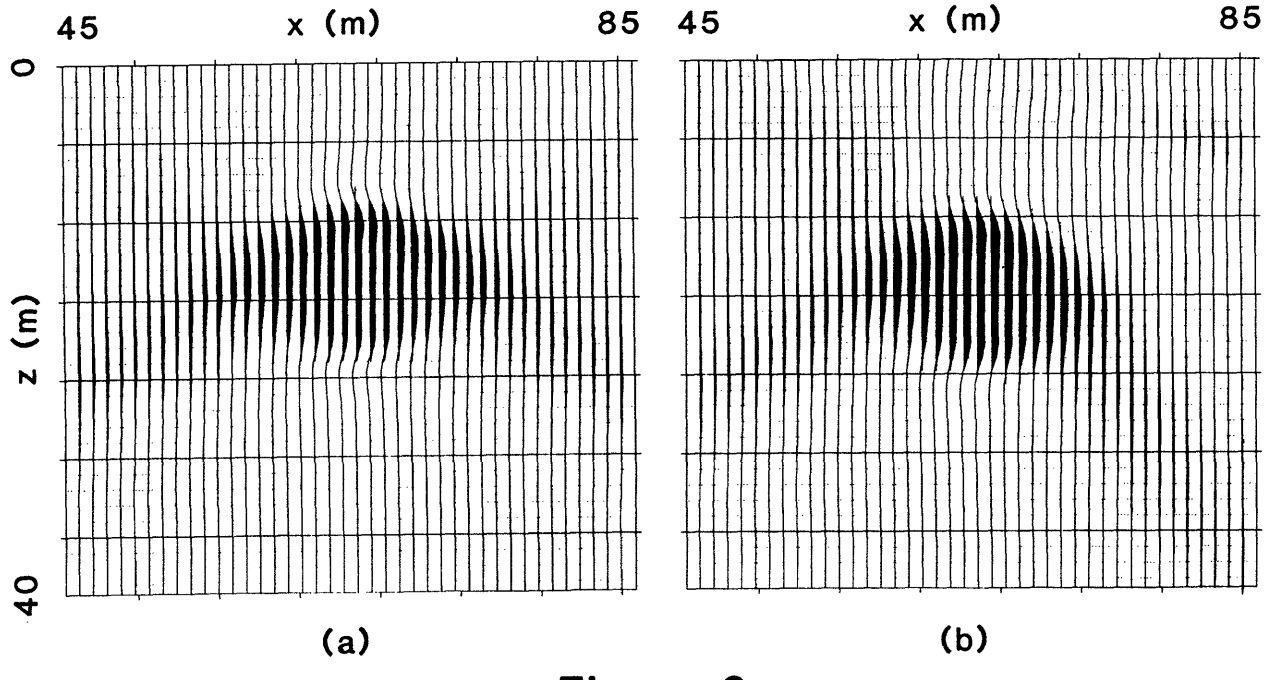

Figure 9

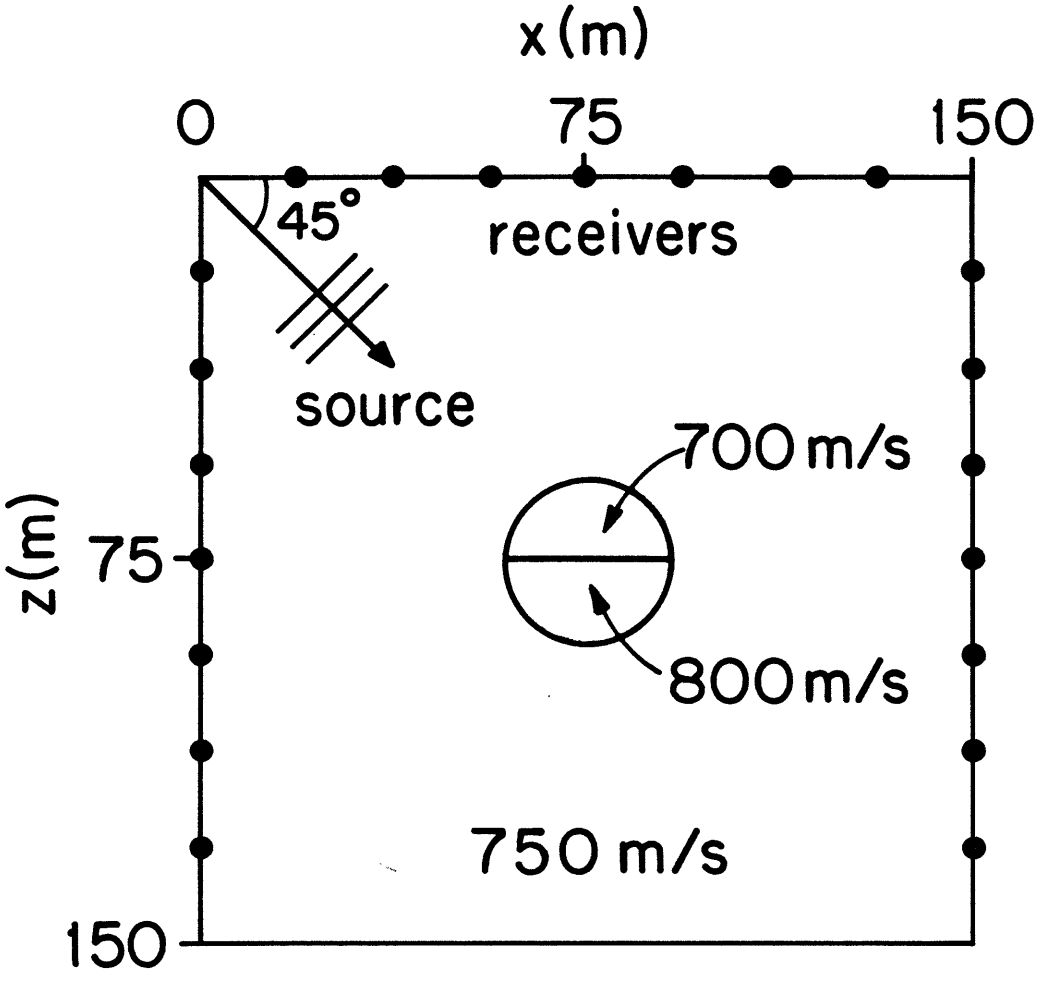

Figure 10

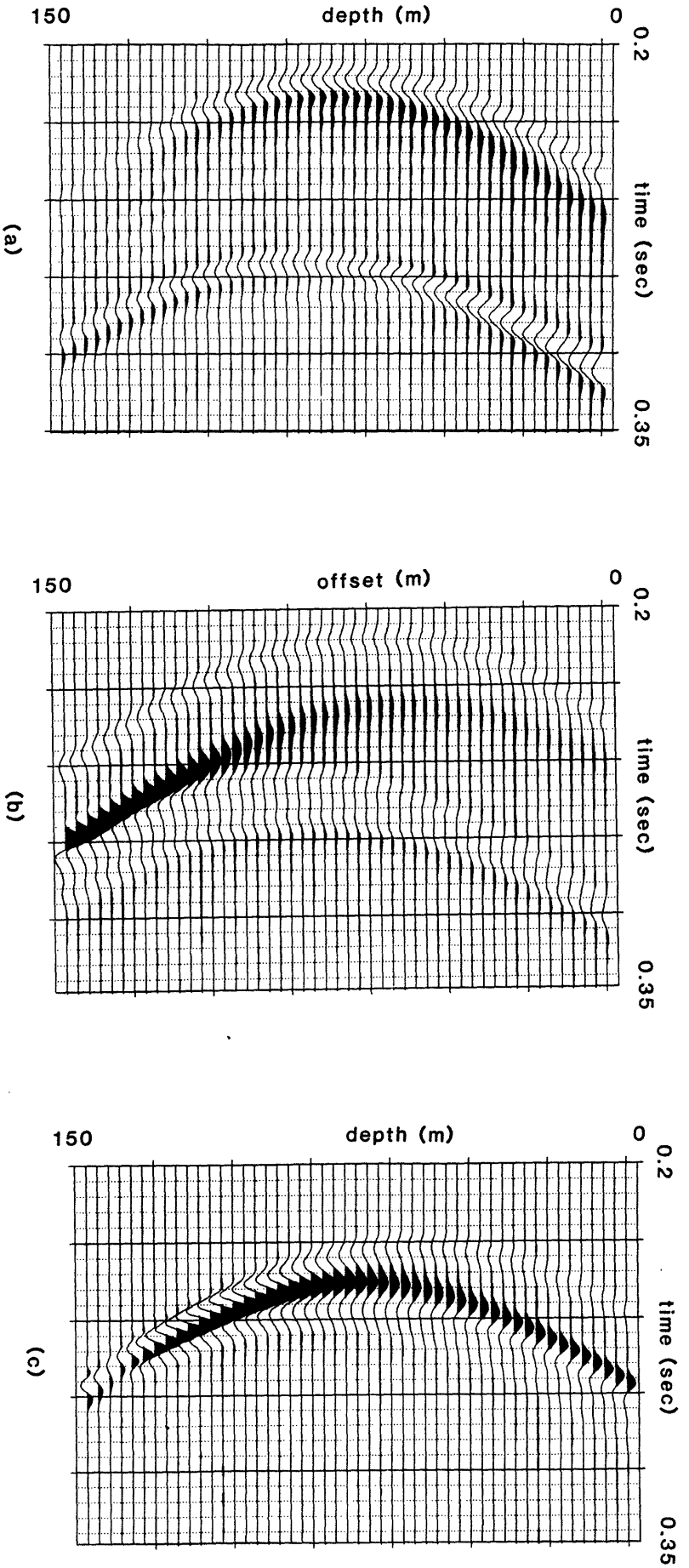
150
depth (m)
0
0.2
time (sec)
0.35
(a)
150
offset (m)
0
0.2
time (sec)
0.35
(b)
150
depth (m)
0
0.2
time (sec)
0.35
(c)

Figure 11

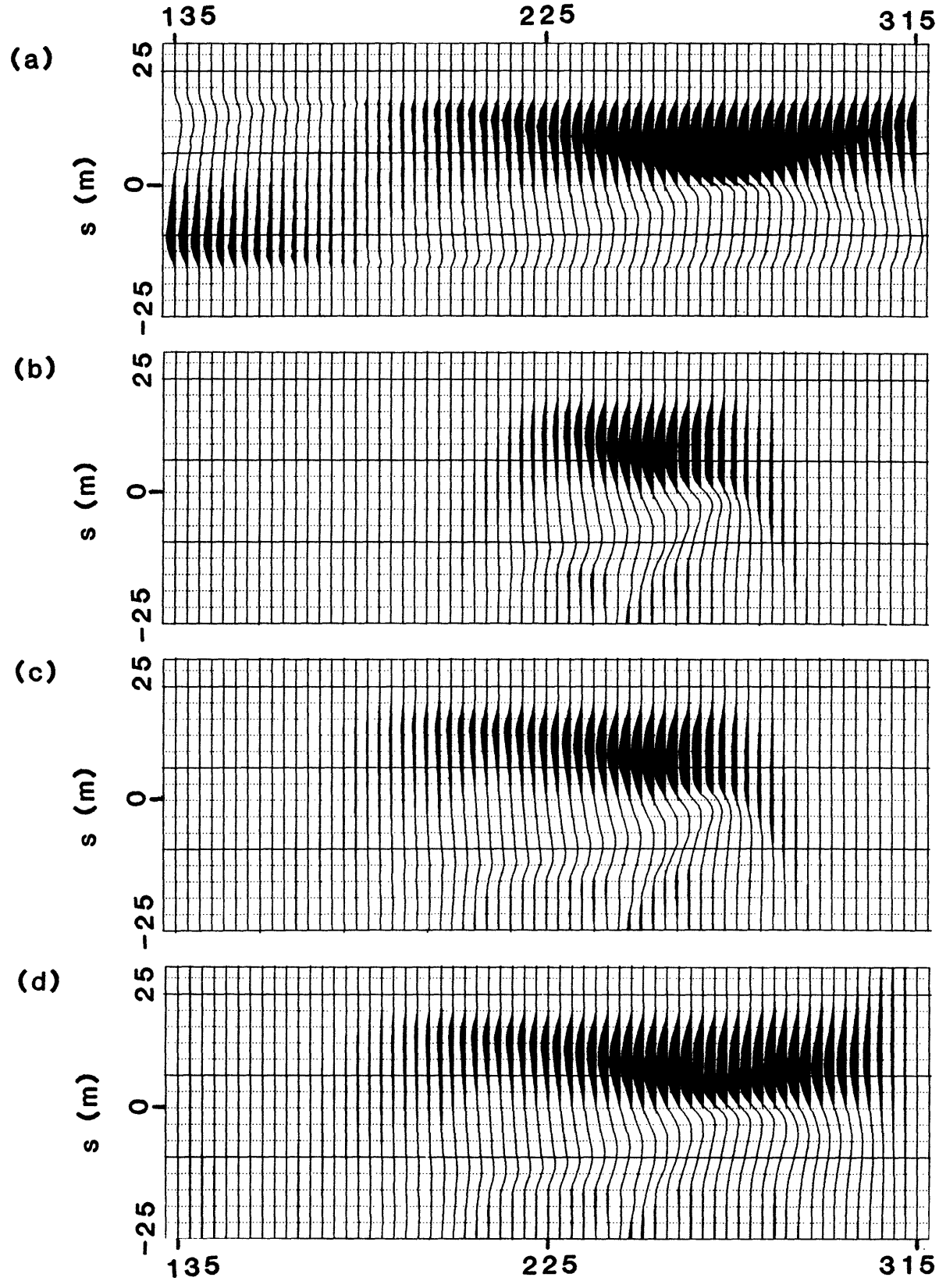

Figure 12

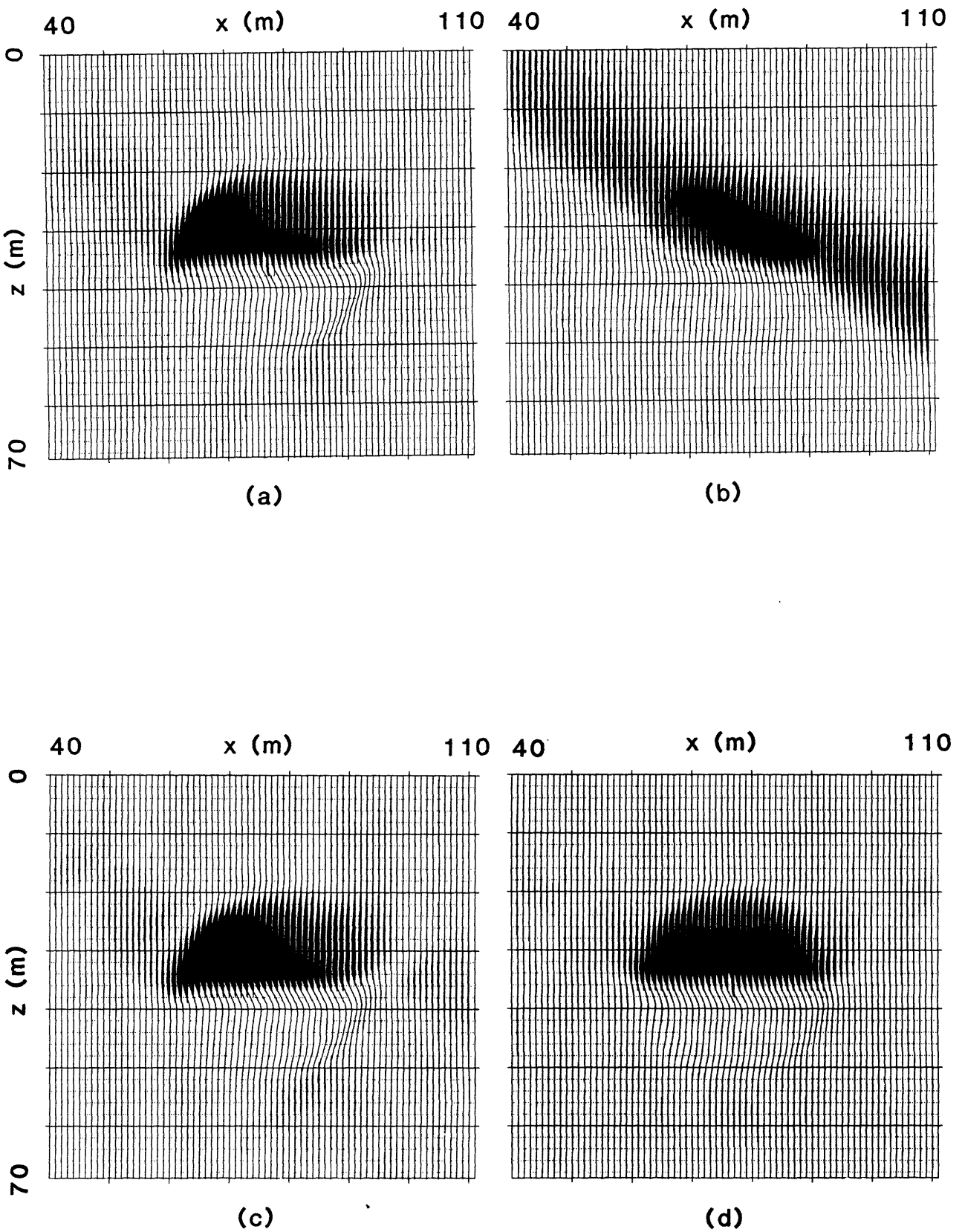

Figure 13

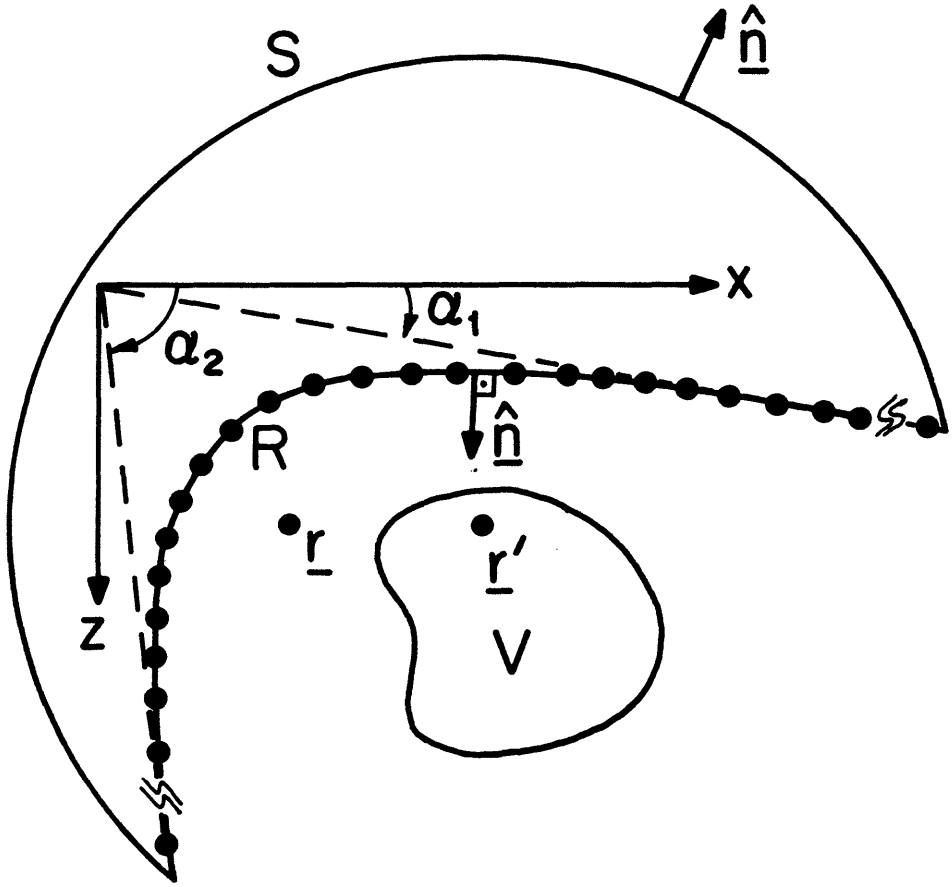

Figure A1